EFFECT OF UTILIZING ROUGHED SURFACES WITHIN A CURVED MICROCHANNEL HAVING CAVITIES ON THE THERMO-HYDRAULIC PERFORMANCE

Khaled M. ALMOHAMMADI[1], Bandar Awadh ALMOHAMMADI[2], Khairy ELSAYED[3], H. A. REFAEY[2,4,*], Mohamed A. KARALI[5,*]

[1]Department of Mechanical Engineering, College of Engineering at Madinah, Taibah University, Saudi Arabia.

[2]Department of Mechanical Engineering, College of Engineering at Yanbu, Taibah University, Yanbu Al-Bahr 41911, Saudi Arabia.

[3]Mechanical Power Engineering Department, Faculty of Engineering - Mataria, Helwan University, MasakenElHelmia P.O., Cairo 11718, Egypt.

[4]Department of Mechanical Engineering, Faculty of Engineering at Shoubra, Benha University, 11629 Cairo, Egypt.

[5]Department of Mechanical Engineering, Faculty of Engineering and Technology, Future University in Egypt, New Cairo, Egypt.

[*] Corresponding authors; Email: mohamedkarali@yahoo.com; mkarali@fue.edu.eg; hassanein.refaey@feng.bu.edu.eg

Curved microchannels with cavities have warranted significant interest from researchers due to their potential to improve the thermo-hydraulic performance of micro-scale hot components. However, there is a scarcity of information concerning the impact of using rough surfaces to such devices for heat transfer enhancement. To this focus, CFD simulations are conducted on a curved microchannel featuring cavities and different surface roughness without identifying any symmetrical planes. The microchannel comprises two curved segments, having a hydraulic diameter (D_h) of 0.3mm. Aluminum serves as a solid material, whereas water functions as a coolant. Reynolds number (Re) varies from 10 to 800. A constant heat flux of 30kW/m² is applied. Three cases with varying surface roughness (K_s/D) are analyzed: 0%, 3%, and 9%. The findings indicated that using rough surfaces is helpful for effective turbulence-inducing through boundary layer disturbing for heat transfer enhancement at low Re. An enhancement in heat transfer of 22.3% is observed, attributable to the roughness of 9% at Re=800, compared to the smooth baseline scenario, while the overall performance improved by about 12.2%. Two correlations are developed as a function of Re and K_s/D for Nusselt and Poiseuille numbers, which are believed to be useful for designers of microchannels.

Keywords*: Rough surfaces; Curved microchannel; Cavity; Heat transfer enhancement; Pressure drop.*

1. Introduction

For researchers aiming to maximize energy exchanges within micro-scale devices for cooling enhancement purposes, studies on microchannel designs are quite crucial [1]. In the case of several micro-scale applications, such as electronics cooling, microfluidics, and energy systems, that involve dissipating high heat flow from very small components, the heat sinks must be greater than the components themselves. However, it is common for hot patches and non-uniform amounts of heat flow to be seen at the heat sink level. When the cooling demand exceeds 100 W/cm^2, it is not feasible to provide sufficient cooling using conventional air or water heat exchangers. Therefore, researchers have been encouraged to create novel heat sinks that can be directly integrated into the heat source's rear to provide consistent heat flux removal. A heat sink of this kind is often constructed using silicon, which is accompanied by a silicon oxide layer to ensure electrical insulation of the component. Using fins in micrometer-sized rectangular channels creates narrow passages that facilitate the efficient evacuation of heat by cycling cool fluid through the microchannels.

The concept of microchannel devices was first elucidated by Tuckerman and Pease [2], as cited by Asadi et al. [3]. Microchannels have gained popularity among researchers due to their high heat transfer coefficients, which have the potential to reach record highs. Additionally, microchannels offer the advantage of low-to-restrained pressure drops when associated with typical air and liquid-cooled systems [4]. An instance of microchannel heat sinks has been shown to cool high-power Laser Diode arrays and achieve a heat flux elimination rate of 500 W/cm^2 [5]. Several investigators have suggested distinct criteria for classifying heat exchanger devices based on the hydraulic diameter (D_h), from micro-scale applications to macro-scale applications to normal-scale applications [6-8].

Different cooling working fluids, from single-phase to two-phase, were employed within microchannels. Researchers have examined single-phase gases within microchannels, such as air, argon, hydrogen, helium, and nitrogen [9-11]. Water was popularly used in microchannel studies [12,13].

Researchers are focusing on the addition of wall structures like cavities and fins to straight microchannels. Such studies focus on their geometry [14, 15], dimensions [16], and orientation [17-19]. However, the commonly used straight microchannels suffer from a problem as the flow becomes regular and the boundary layer thickens, resulting in poor heat transfer performance along the streamwise direction. As a result, curved microchannels have been developed and recognized as an effective means of improving hydraulic and thermal performance by disrupting the boundary layer, inducing secondary flows or Dean vortex, due to centrifugal forces inside the curved section [20, 21], and promoting chaotic advection [22].

A curved microchannel consists of a curved portion with a certain curvature radius (R) coupled to two straight sections on each side. Their use encompasses the fields of bioengineering [23], energy management [24], and microfluidic systems [25, 26], demonstrating their diversity and efficacy. The following are related research studies that focus on investigating curved microchannels. Khoshvaght-Aliabadi et al. [27] examined the impact of several cross-section geometries on the efficiency of a corrugated micro heat sink. The study considered four cases: uniform, convergent, divergent, and hybrid. Zhang et al. [28] investigated the flow and heat transfer properties in microchannels with wavy and curved wavy geometries. Additional research has shifted towards the development of curved microchannels that are combined with wall constructions. Utilizing the combined advantages of secondary flows and disruptions in wall construction to improve thermal efficiency. The study of Chandratilleke et al. [29] examined the flow instability caused by helicity functions and unfavorable pressure gradients on the outer wall. Liu et al.[30] introduced the concept of Dean instability to investigate sinusoidal microchannels. Introducing wall features such as cavities, ribs, and nano-wires is acknowledged as an efficient approach to enhancing fluid mixing in curved microchannels [31]. The curved microchannel with wall voids is optimal for achieving efficient convective heat transfer. Liu et al. [32] performed a study on serpentine microchannels, including fan-shaped cavities, primarily investigating the dimensions and morphology of the wall structures.

The recent research by Li et al. [1] highlights cavities as an optimal option for wall construction in curved microchannels. Its uncomplicated production, cost-effectiveness, and structural stability further support this decision. The researchers conducted a quantitative analysis to examine how the distribution of cavities affects the flow dynamics and heat transmission in curved microchannels. Four traditional cavity configurations were employed: symmetrical, staggered, exterior-only, and interior-only, along with a microchannel without any cavities for comparative purposes. Their findings showed that the staggered distribution of cavities significantly decreases flow resistance, which is supported by its high cavity throughput ratio. The distribution of the cavity in a symmetrical manner exhibits the highest level of thermal efficiency, resulting in the attainment of the maximum thermal performance assessment. In their subsequent study, Li et al. [33] explored the curvature ratio's impact on flow and heat transmission. Three different curvature radii were employed: 1 mm, 3 mm, and 5 mm. Their findings demonstrated that greater curvatures display enhanced overall thermal efficiency, although at the expense of increased flow resistance within a manageable range. Nevertheless, the capacity to create bigger curvatures is limited by factors such as the accuracy of machining, the stability of mechanical components, and the expenses associated with production.

Roughening the microchannel heat transfer surfaces was proposed as a passive technique for heat transfer enhancements in such devices [25] as it helps to accelerate the transition from laminar to turbulent, which makes it an effective method for turbulence-inducing through disturbing the boundary layer at low Re. However, in addition to the difficulty of measuring roughness from small cross sections like microchannels, there are still difficulties in fabricating such rough surfaces, particularly at such a small scale. As a result, the literature has limited investigations on surface roughness in microchannels. Compared to challenging experimental research, this presents numerical simulations (CFD) as a viable and efficient method of obtaining a precise understanding of microchannel flows at a lower cost [34].

In a notable investigation conducted by Mandev and Manay [35], tests were conducted to examine the impact of surface roughness on heat transfer in numerous straight microchannels made of stainless steel. The research specifically focused on the combined impacts of natural and induced convection on the overall heat transfer process. The studies used microchannel heat sinks with three distinct surface roughness values (K_s): 1.1, 1.8, and 3.0 μm. These heat sinks also had three different microchannel widths of 300, 500, and 700 μm, and two dissimilar heights: 300 and 450 μm. The microchannel heat sink was subjected to a steady heat flux on its backside surface using pure water as the working fluid. The trials were included within a Reynolds number range of 10–80 to guarantee mixed convective conditions. Their findings demonstrated that an augmentation in hydraulic diameter decreased the impact of surface roughness on the total heat transmission. The influence of surface roughness on mixed convection in a microchannel with constant width and height is only noticeable when the Grashof number rises. The most optimal heat transfer outcomes were achieved with the microchannel with the narrowest cross-section of 300 × 300 μm^2 and the maximum roughness value of 3.0 μm.

Based on the preceding information and concluding remarks, the present study was suggested to provide more details to ensure the validity of using rough surfaces beside body cavities for effective turbulence-inducing, even at low Re values, aiming to enhance the heat transfer and consequently improve the cooling of micro-scale devices. This gives the potential of the current paper for better design and manufacture of microchannels, especially when there are very limited papers found in the literature regarding this issue, due to many difficulties in measuring roughness from small cross sections like microchannels and their fabrication.

2. Methods

2.1 Geometrical parameters and considered domains

Fig. 1 shows the specifications of the studied geometry, a curved multiple-turn microchannel with cavities, with full dimensions in mm. The dimensions are taken as found by Li et al. [1, 33]. However, the geometry is modified to include two curved sections as a proposed option for more practical usage. Two distinct domains can be identified: solid domain and passing fluid domain. The physical model of the microchannel comprises two curved sections of 1 mm curvature radius (R) and three straight sections; two of them are equal in length (L = 20 mm), and the third one is the connecting part between the two curvature sections with a length of 18.45 mm. A total of 10 wall cavities are grooved in the solid body. Two cavities are located at the end of the straight section in connection with the curvature sections, and the remaining three cavities are evenly distributed along the curved circumferential [1, 33]. All cavities have the same width (w_{cav}) of 0.3 mm and a depth (h_{cav}) of 0.1 mm. The height of both the cavities and the fluid channel (h) is the same (0.3 mm). The total height (H) of the microchannel is 0.35 mm, and the width (W) is 1.1 mm. The length of the straight sections is enough to ensure fully developed conditions before entering the curved sections. An important parameter to describe fluid flow in a channel is the hydraulic diameter (D_h), which can be computed based on Eq. (1). The hydraulic diameter (D_h) of the present channel geometry is 0.3 mm. All geometrical parameters with full descriptions and values are listed in Table 1.

$$D_h = \frac{2hw}{h+w} \tag{1}$$

Table (1): Geometrical parameters

Geometry parameter	Description	Value in mm
R	Curvature radius	1.0
L	Straight section length	20
W	Solid-body width	1.1
H	Solid-body height	0.35
w	Fluid channel width	0.3
h	Fluid channel height	0.3
D_h	Hydraulic diameter	0.3
w_{cav}	Cavity width	0.3
h_{cav}	Cavity depth	0.1

2.2 Used materials and boundary conditions

Aluminum is used here as the material for the solid microchannel body, and water acts as the working fluid. Water enters and leaves the microchannel, as displayed in Fig. 1 (a). The fluid inlet is defined as a "velocity inlet" that corresponds to the studied Reynolds number range from 10 to 800 [1], including 13 points (10, 20, 40, 60, 80, 100, 200, 300, 400, 500, 600, 700, and 800). Such a range of Reynolds number is sufficient to cover a wide range of applications using microchannels. The relation between the velocity and Reynolds number is demonstrated in Eq. (2), and all fluid properties are recorded in Table 3. The fluid outlet is defined as a "pressure outlet" with a zero value corresponding to the atmospheric pressure (fully developed flow). The upper surface of the flowing fluid is sealed, preventing any transfer of heat. A continuous heat flux (q) density of 300,000 W/m^2 is employed on the bottom surface of the solid body, while the remaining surfaces of the solid body are thermally insulated from the external environment.

Three cases with different surface roughness at the microchannel inner surfaces are examined. This surface roughness is expressed by the relative roughness (K_s/D_h) in many publications [36, 37, 38]. From the smooth base case (K_s/D_h=0) to K_s/D_h= 3 % and K_s/D_h= 9 %. All simulation specifications are found in Table 2. Where K_s is the sand grain roughness in µm, and D_h is the hydraulic diameter.

$$\mathrm{Re} = \frac{\rho \,\mathrm{v}\, D_h}{\mu} \tag{2}$$

Table (2): Simulation specifications

Re	Roughness presentation	
	Relative (K_s/D_h) in %	Sand grain (K_s) in µm
10-20-40-60-80-100-200-300-400-500-600-700-800	0*	0*
	3	9
	9	27

D_h - hydraulic diameter = 0.3 mm

* smooth base case

Table (3): Working fluid properties

Property	Value
Density (ρ)	998 kg/m^3
Specific heat (c_p)	4182 J/kg.K
Thermal conductivity (k)	0.6 W/m^2. K
Dynamic viscosity (µ)	0.001003 Pa.s

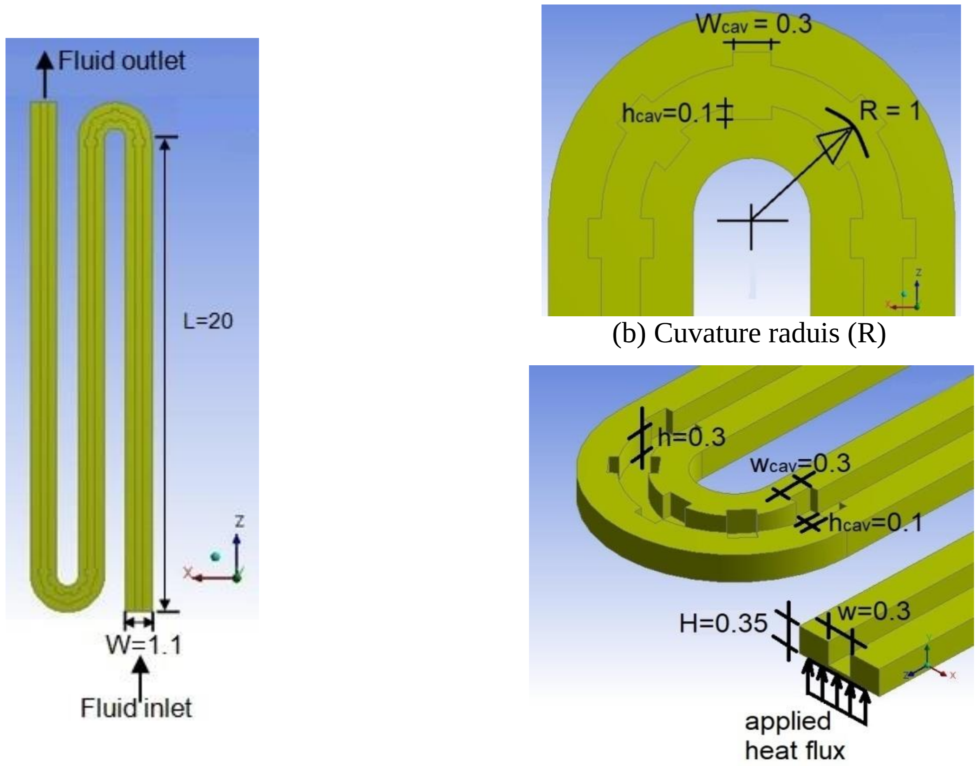

(b) Cuvature raduis (R)

(a) Geometry overview

(c) Zoom in isometry view

Figure 1. Specifications of the studied geometry: curved multiple-turn microchannel with cavities (dimensions are in mm).

The model encompasses the fundamental equations governing mass, momentum, and energy transmission as [39]:

Continuity equation

$$\frac{\partial u_i}{\partial x_i} = 0 \qquad (i = 1, 2, 3) \tag{3}$$

Momentum equation

$$\frac{\partial}{\partial x_j}\left(\rho u_i u_j\right) = -\frac{\partial p}{\partial x_i} + \frac{\partial}{\partial x_i}\left[\mu\left(\frac{\partial u_i}{\partial x_j} + \frac{\partial u_j}{\partial x_i}\right)\right], \ (i, j = 1, 2, 3) \tag{4}$$

Energy equation

$$\frac{\partial}{\partial x_i}\left(\rho u_i c_p T\right) = \frac{\partial}{\partial x_i}\left(k\frac{\partial T}{\partial x_i}\right) + \mu\left[2\left(\frac{\partial u_i}{\partial x_i}\right)^2 + \left(\frac{\partial u_i}{\partial x_j} + \frac{\partial u_j}{\partial x_i}\right)^2\right], \ (i, j = 1, 2, 3) \tag{5}$$

This study uses ANSYS-CFX R18.0 CFD solver code. "SIMPLE" pressure-velocity coupling was used. For pressure, second-order upwind discretization was used. Second-order upwind discretization was used for momentum, turbulent kinetic energy, and dissipation rates. Problem convergence was based on a residual mean square. Solutions were accepted at residual goals of 10^{-6}. All simulations were done without symmetry planes.

2.3 Meshing specifications and independent study

This CFD research used ANSYS-ICEM Mesh R18.0 [40] with non-uniform grid spreading. A computational domain mesh setup overview is shown in Fig. 2. Six distinct mesh densities were examined at Re = 450 for the grid independence investigation to choose the best mesh. The number of elements used is 228657, 293988, 328201, 599565, 1009966, and 1495523. The selection criterion is based on the minimum deviation in measuring the fluid inlet pressure. It is found that the pressure is more sensitive to the fluid grid size. The deviations of these measurements are found as: 4.52, 2.52, 1.55,0.11, and 0.12, respectively. Thus, it is reasonable to use the mesh setting found in mesh number "5" for the simulations that have been studied.

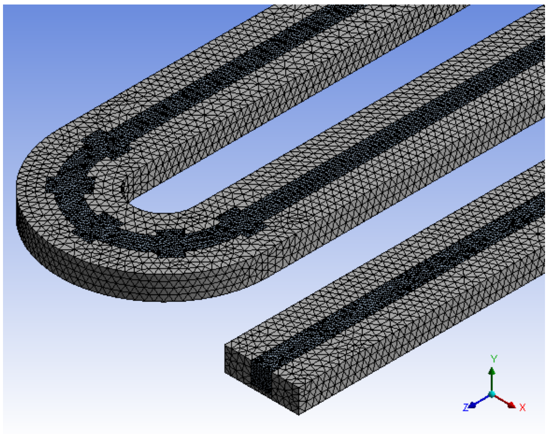

Figure 2. Overview of the meshing in the studied domains.

2.4 Model validation

To assess the reliability and accuracy of the existing computational model and methodologies, the numerical results of Nu are compared with those reported by Li et al. [19]. The physical model comprised a microchannel with dimensions: length L = 40 mm, width W = 1 mm, and height H = 0.5 mm. The microchannel comprised an entrance segment of length L_{in} = 0.8 mm, a central section, and an exit segment of length L_{out} = 1.08 mm in the flow direction. Symmetrical fins or chambers were developed on the lateral aspects of the central region. The fin width and spacing measured I_f =0.12 mm and l_s = 0.5 mm, respectively. The fluid domain's cross-sectional area measured 0.3 x 0.3 mm^2. The upper boundary of the fluid domain was sealed, inhibiting mass and heat transfer. A continuous heat flux of 30 kW/m^2 was applied to the bottom surface of the solid, with the remaining walls being thermally insulated. Silicon was selected as the solid channel, and water was utilized as the fluid. The Reynolds number was defined within the range of 25 to 500. The validation relied on a singular example featuring a fin height of 0.04 mm, an aspect ratio of 3, and an angle of 90 degrees. Figure 3 presents the validation findings, illustrating the concordance between the two outcomes.

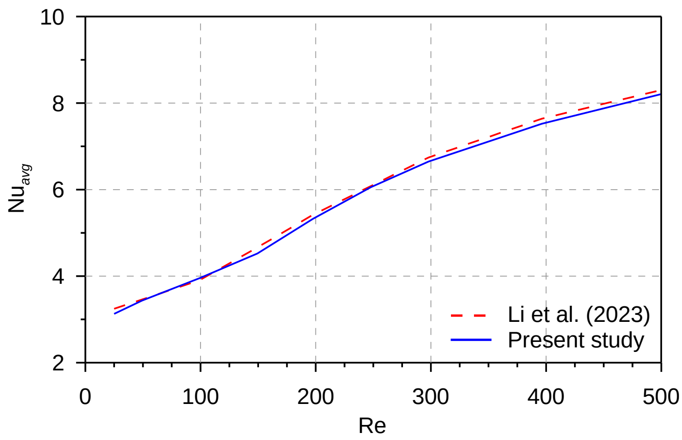

Figure 3. CFD validation with literature.

3. Equations

The heat transfer process of the presently studied problem is simply illustrated in Fig. 4. The applied heat flux is used to heat the bottom surface of the solid body through the heating area (A_h). At steady state conditions and with the assumption of perfect insulation for outer microchannel surfaces. This amount of heat is conducted to the solid body surfaces that face the moving fluid (A_s). The heat energy is then transferred by convection to the passing cooling fluid under the assumption of radiation neglect. Hence, the temperature of the fluid tends to rise from the cold inlet (T_{in}) to the hot outlet (T_{out}). Such a heat balance can be expressed as follows.

$$Q = q\ A_h = h_{conv}\ A_s\ (T_{s,avg} - T_{f,avg}) \tag{6}$$

Where Q is the heat transfer rate in Watt, q is the applied heat flux, Ah is the solid bottom heating area, hconv is the average convection heat transfer coefficient, As is the solid-fluid contact area, Ts,avg is the average solid surface temperature, and $T_{f,avg}$ is the fluid average temperature.

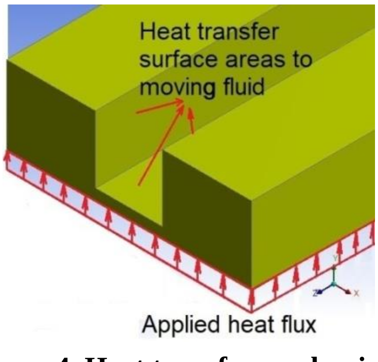

Figure 4. Heat transfer mechanism.

$$h_{conv} = \frac{q\ A_h}{A_s\ (T_{s,avg} - T_{f,avg})} \tag{7}$$

Nusselt number (Nu) is an important dimensionless group that represents the enhancement in heat transferred due to convection by fluid motion. It is considered here for the evaluation of the current problem's thermal performance. The average Nusselt number can be evaluated as:

$$\text{Nu} = \frac{h_{conv}\ D_h}{k} \tag{8}$$

The fluid pressure drop is a main parameter that controls the fluid pumping power. The evaluation of the studied problem based on the pressure drop is verified by employing the Poiseuille number (Po) that can be expressed as [1]:

$$\mathrm{Po} = \frac{2\Delta p \, D_h}{\rho \, L_{total} \, \mathrm{v}^2} \, \mathrm{Re} \tag{9}$$

Where Δp is the difference in pressure between the fluid inlet and outlet, and L_{total} is the total length of the fluid path.

Finally, an overall performance evaluation (OPE) parameter is presented for the overall performance [1]:

$$\mathrm{OPE} = \frac{\mathrm{Nu/Nu}_{smooth}}{\left(\mathrm{Po}/\mathrm{Po}_{smooth}\right)^{1/3}} \tag{10}$$

Nu_{smooth} corresponds to the smooth case (base case), Po is the Poiseuille number for a studied case and Po_{smooth} is the Poiseuille number for the corresponding smooth case (base case). The higher the OPE, the more it verifies the main target of this study, as it yields the significance of heat transfer improvement using a specified microchannel design over the drawbacks from pressure drop and pumping power penalties.

4. Results and Discussions

The present study focuses on the enhancement of the heat transfer rate with an optimal pumping power. This is accomplished by employing different surface roughnesses on the studied geometry. The performance is assessed by discussing the results of Nu, Po, and OPE. In the following subsections, all these performance parameters are presented for a specified case as normalized by the corresponding results of the smooth case (base case).

Fig. 5 depicts the variation of normalized Nu with Re for the two cases studied, namely, roughness 3% and 9%. The first observation from Fig. 5 is that all the values are above one. This means heat transfer enhancement is possible when using rough surfaces over the base case of smooth surfaces. This has been proved by previous research on other geometries [35]. Rough surfaces are found helpful in promoting turbulence induction through boundary layer disturbances, even at low Re values. Consequently, it increases the surface side convection heat transfer coefficient and Nusselt number. Moreover, it could be deduced that the enhancement in Nu is more pronounced for higher Re values. This helps to effectively cool the microchannel’s surface temperature, as will be discussed later in the temperature gradient subsection. Also, this is consistent with the results from previously published research [1, 33]. As an example, at Re = 800, the surface roughness of 9% ensures an enhancement in the heat transferred by about 22.3%, while the surface roughness of 3% achieved an enhancement of about 8.2%.

The variation of the normalized Po with the Re is demonstrated in Fig. 6. Back to Eq. 9, the Po is a good choice to describe the relation between the fluid pressure drop and velocity at the constant fluid properties and geometry. It could be deduced from Fig. 6 that all the values are above unity, which indicates a higher-pressure gradient when employing surface roughness over the smooth base case. This implies that higher pumping power is required. Moreover, this high pumping power is more pronounced for the higher values of Re, indicating the main drawback when increasing the surface roughness. As an example, the required pumping power is increased by about 29.3% and 10% for the cases, roughness 10.2% and roughness 3% respectively, at Re = 800.

A final judgment of the present study of employing different surface roughness is based on the OPE parameter as presented in Fig. 7. It can be seen from Fig. 7 that the OPE increases with Re, due to the enhancement of the Nu over the drawbacks from increasing the pressure drop. However, this enhancement in the OPE is more pronounced for the higher surface roughness of 9%. As an example, from Fig. 7, an increase in the OPE value with an average of 12.2% for the case of 9% surface roughness is reported at Re = 800. In contrast, a lower increase is noted for the 3% roughness case with an average value of 4.8% at the same Re. Hence, a conclusion can be drawn here that, for better overall performance, it is recommended to use heat transfer devices with higher surface roughness and higher values of Re. This general conclusion is confirmed by previous studies on other straight microchannel geometries [35, 41].

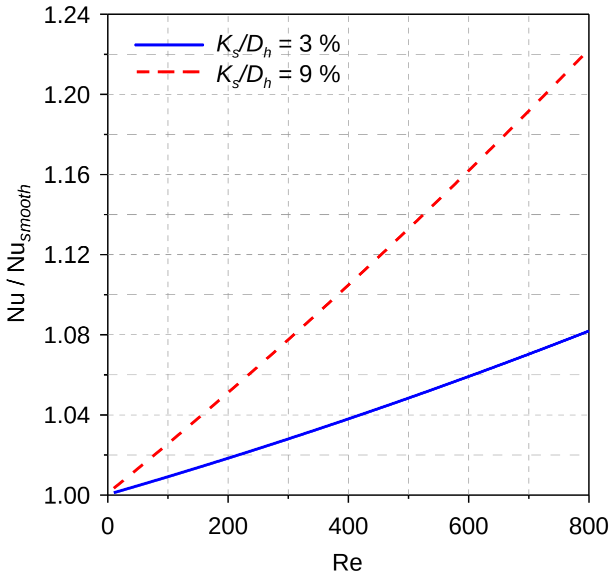

Figure 5. The variation of the normalized Nu number with the Re number range.

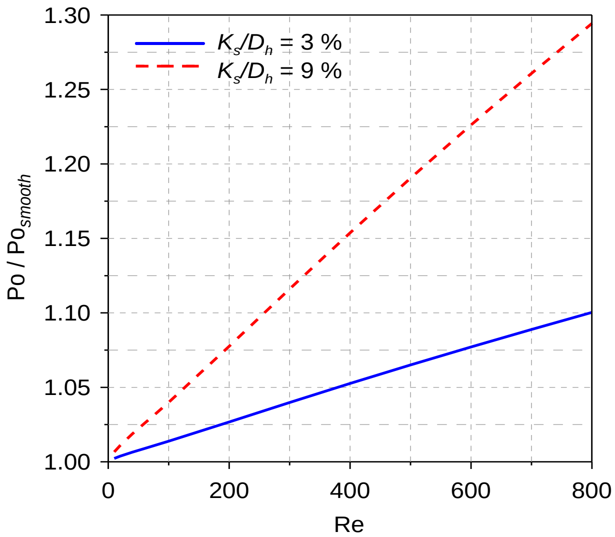

Figure 6. The variation of the normalized Po number with the Re number range.

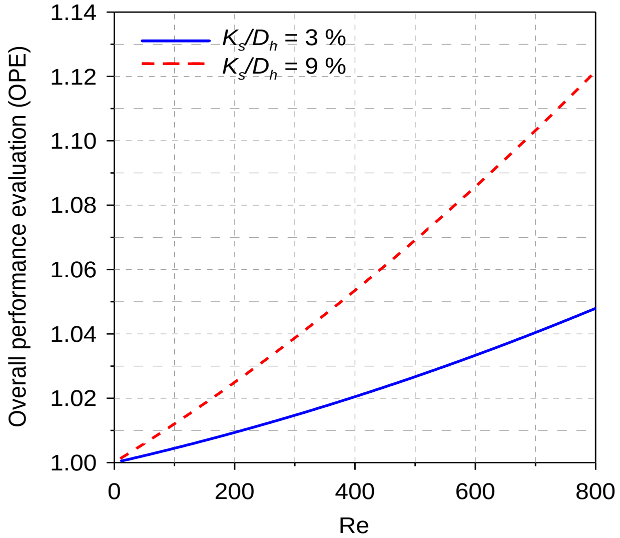

Figure 7. The variation of the overall performance evaluation (OPE) with the Re number range.

Two correlations were developed by gathering all the resulting data as a function of Re and K_s/D. One correlation is found for the Nu/Nu$_{smooth}$ while the other is for the Po /Po$_{smooth}$, as given in the following:

$$\frac{\mathrm{Nu}}{\mathrm{Nu}_{smooth}} = 0.943 + 0.000164\,(\mathrm{Re}) + 1.006\left(\frac{K_s}{D}\right) \tag{11}$$

$$\frac{\mathrm{Po}}{\mathrm{Po}_{smooth}} = 0.909 + 0.00024\,(\mathrm{Re}) + 1.564\left(\frac{K_s}{D}\right) \tag{12}$$

It is worth noting that the above two correlations are valid for the ranges of studied geometrical and varied parameters within the present study. The maximum error of the calculations from the two equations is 2.18 % and 3.25 %, respectively.

For more discussion and verifications of the preceding results from the present study, selected contours from the temperature and the velocity gradients are demonstrated in Fig. 8 and Fig. 9, respectively. For the case of 9% surface roughness at Re values of 10, 500, and 800. It can be observed from Fig. 8 that the highest temperatures attained by the passing fluid are in the case of a lower Re value of 10 due to a lower fluid flow rate, which results in the cooling degradation of the microchannel surface temperature. Clearly, it is shown from Fig. 9 that the remarkably varied velocity gradients correspond to different Re values. Also, it is clearly demonstrated that the increase in the velocity gradients inside the curvature sections is due to the induced centrifugal force causing the secondary flow or Dean vortex.

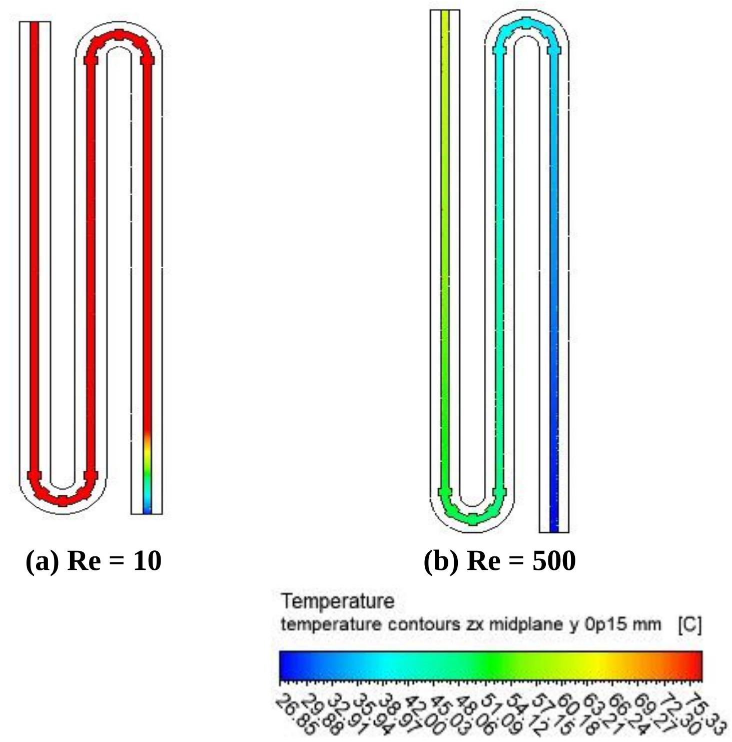

Figure 8. Selected temperature contours at ZX mid-plane for the cases of roughness 9%.

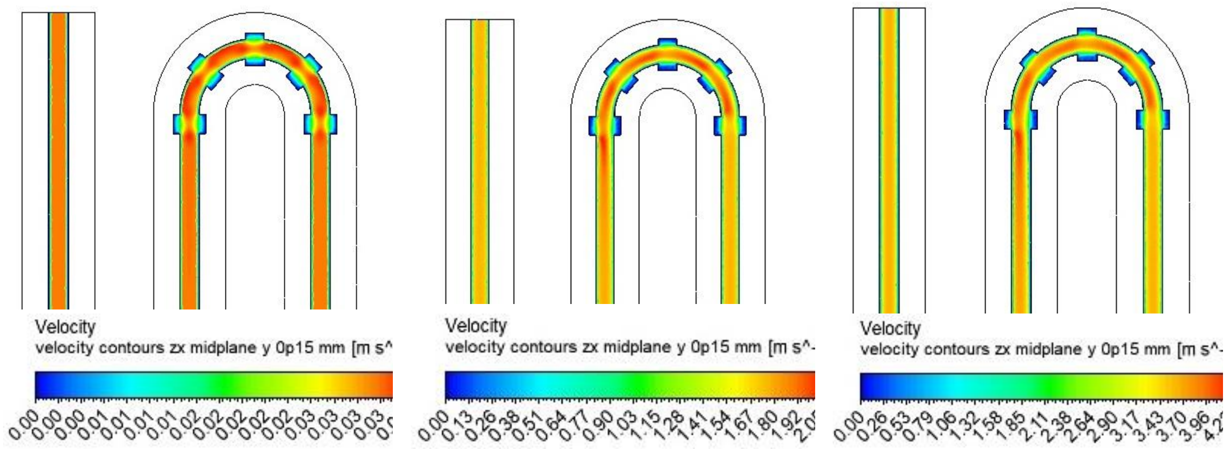

(a) Re = 10 **(b) Re = 500** **(c) Re = 800**

Figure 9. Selected velocity contours at ZX mid-plane for the cases of roughness 9 %.

5. Conclusions

In this work, many CFD simulations are carried out to simulate a curved multiple-turn microchannel with cavities at different surface roughness values, without using any symmetrical planes. The physical model of the microchannel is comprised of two curved sections of 1 mm curvature radius (R) and three straight sections; two of them are equal in length (L = 20 mm). A total of 10 wall cavities are grooved in the solid body. Two cavities are located at the end of the straight section in connection with the curvature sections, and the remaining three cavities are evenly distributed along the curved circumferential. All cavities have a width (w_{cav}) of 0.3 mm and a depth (h_{cav}) of 0.1 mm. The height of both the cavities and the fluid channel (h) is the same at 0.3 mm. The total height (H) of the microchannel is 0.35 mm, and the width (W) is 1.1 mm. The hydraulic diameter (D_h) of the present channel is 0.3 mm. Aluminum is used as the solid material, and water acts as the passing fluid. The studied range of Reynolds number is from 10 to 800, including 13 points. A constant heat flux (q) density is imposed on the bottom of the solid body at a rate of 30 kW/m^2. Three cases with different surface roughness at the microchannel inner surfaces are examined, expressed by the relative roughness (K_s/D_h), from the smooth base case (K_s/D_h=0) to K_s/D_h= 3 % and K_s/D_h= 9 %.

The result from the present study is assessed in terms of Nusselt number (Nu), Poiseuille number (Po), and an introduced parameter representing the overall performance evaluation (OPE). The results confirmed the augmentation of heat transfer due to the use of rough surfaces. That is due to the turbulence induced through the disturbance found in the boundary layer, even at low Re values. Such an enhancement is also associated with the higher Re range. With some drawbacks on the higher pumping power required. At Re=800, the surface roughness of 9% ensures an enhancement in the heat transferred by about 22.3%, while the drawbacks from the pumping power increased by about 29.3%.

A final judgment of the present study is based on the OPE parameter that emphasizes the overall enhancement due to the increase in both surface roughness and Re values. An increase in the OPE value of about 12.2% for the 9% surface roughness case compared to the smooth base case is reported at Re of 800. Hence, a final conclusion from the present study can be drawn that for better overall performance, it is recommended to use heat transfer devices with higher surface roughness and higher values of Re. Previous studies on other geometries confirm this general conclusion. Two correlations were developed for the Nu/Nu_{smooth} and for the Po/Po_{smooth}, as a function of Re and K_s/D.

The present study, along with related studies found in the literature, has a potential benefit for microchannel manufacturers. Manufacturing cavities and rough surfaces at such a micro scale presents challenges. Future work should examine different coolant fluids for heat transfer enhancement.

Nomenclature

Symbols

A_h	heating area, [m^2]
A_s	contact areas between fluid and solid, [m^2]
c_p	fluid specific heat coefficient, [Jkg^{-1}K^{-1}]
D_h	hydraulic diameter, [mm]
H	microchannel total height, [mm]
H	fluid channel height, [mm]
h_{cav}	cavity depth, [mm]
h_{conv}	average convection coefficient, [Wm^{-2}K^{-1}]
K	fluid thermal conductivity, [Wm^{-1}K^{-1}]
K_s	sand grain roughness, [µm]
L	straight section length, [mm]
Nu	Nusselt number
OPE	overall performance evaluation

Subscripts

avg	Average
conv	Convection
f, avg	fluid average
In	Inlet
out	Outlet
s, avg	solid average
smooth	Smooth
total	Total

Greek letters

ρ	fluid density, [kg/m^3]
Δ	Difference
μ	fluid dynamic viscosity, [Pa.s]

P	pressure, [Pa]
Po	Poiseuille number
Q	heat transfer rate, [W]
Q	heat flux, [Wm^{-2}]
R	curvature radius, [mm]
Re	Reynolds number
T	temperature, [K]
V	velocity, [m/s]
W	microchannel width, [mm]
W	fluid channel width, [mm]
w_{cav}	cavity width, [mm]

References

[1] Li, M.; Gao, X.; Li, H.; Xu, T., A quantitative study on the influence of cavity distributionon flow and heat transfer characteristics in curved microchannels introducing the cavity throughput ratio. Applied Thermal Engineering 241 (2024). 122388. https://doi.org/10.1016/j.applthermaleng.2024.122388

[2] Tuckerman, D.B.; Pease, R.F., High performance heat sinking for VLSI. IEEEElectron. Dev. Lett. EDL 2 (1981) 126–129.

[3] Asadi, M.; Xie, G.; Sunden, B., A review of heat transfer and pressure drop characteristics of single and two-phase microchannels. International Journal of Heat and Mass Transfer 79 (2014) 34–53. http://dx.doi.org/10.1016/j.ijheatmasstransfer.2014.07.090

[4] Viday, A.V.; Soshelev, S.B.; Reznikov, G.V.; Kharitonov, V.V.; Cheremushkin, S.V., Thermophysical design of the parameters of a computer board with a microchannel cooling system. J. Eng. Phys. Thermophys. 64 (1) (1993) 80–86.

[5] Mundinger, D.; Beach, R.; Benett, W.; Solarz, R.; Krupke, W.; Staver, R.; Tuckerman, D., Demonstration of high performance silicon microchannel heat exchangers for laser diode array cooling, Appl. Phys. Lett. 53 (12) (1988) 1030–1032. http://dx.doi.org/10.1063/1.100055

[6] Mehendale, S.S.; Jacobi, A.M.; Ahah, R.K., Fluid flow and heat transfer at micro and meso-scales with application to heat exchanger design, Appl. Mech. Rev. 53 (2000) 175–193.

[7] Kandlikar, S.G.; Grande, W.J., Evolution of microchannel flow passages thermo hydraulic performance and fabrication technology. Heat Transfer Eng. 24 (2003) 3–17. http://dx.doi.org/10.1080/01457630304040

[8] Chen, S.; Liu, Z.; Wang, B.; Li, P., Heat transfer enhancement and temperature uniformity improvement of microchannel heat sinks with twisted blade-like fins. Case Studies in Thermal Engineering 52 (2023) 103788. https://doi.org/10.1016/j.csite.2023.103788

[9] Pfahler, J.; Harley, J.; Bau, H.H.; Zemel, J.N., Liquid and gas transport in small channels. Proceedings of the ASME DSC, 31 (1990) 149–157.

[10] Zhang, X.; Liu, J.; Liu, Y.; Zhang, G., Optimized Design and Testing of Enhanced Heat

Transfer Secondary Micro-Channels on the Surface of Fuel Cell Bipolar Plate Flow Channels. *Energies*. 18(6) (2025) 1459.
https://doi.org/10.3390/en18061459

[11] Asako, Y.; Nakayama, K.; Shinozuka, T., Effect of compressibility on gaseous flows in a micro-tube. Int. J. Heat Mass Transfer 48 (2005) 4985–4994.
doi:10.1016/j.ijheatmasstransfer.2005.05.039

[12] Qu, W.; Mudawar, I., Experimental and numerical study of pressure drop and heat transfer in a single-phase micro-channel heat sink. Int. J. Heat Mass Transfer 45 (12) (2002) 2549–2565.

[13] Shen, S.; Xu, J.L.; Zhou, J.J.; Chen, Y., Flow and heat transfer in microchannels with rough wall surface. J. Energy Convers. Manage. 47 (2006) 1311–1325.
doi:10.1016/j.enconman.2005.09.001

[14] Abdoli, A.; Jimenez, G.; Dulikravich, G.S., Thermo-fluid analysis of micro pin-fin array cooling configurations for high heat fluxes with a hot spot. Int. J. Therm. Sci. 90 (2015) 290–297.
http://dx.doi.org/10.1016/j.ijthermalsci.2014.12.021

[15] Rajalingam A.; Chakraborty, S., Effect of shape and arrangement of micro-structures in a microchannel heat sink on the thermo-hydraulic performance. Applied Thermal Engineering 190 (2021) 116755.
https://doi.org/10.1016/j.applthermaleng.2021.116755

[16] Wang, H.; Fu, T.; Wang, J.; Zhang, F.; Zhang, K.; Deng, X., Study on heat transfer performance of fin-and-tube heat exchanger with elliptical fins. J. Energy Storage 56 (2022) 105956.
https://doi.org/10.1016/j.est.2022.105956

[17] Jia, Y.; Xia, G.; Li, Y.; Ma, D.; Cai, B., Heat transfer and fluid flow characteristics of combined microchannel with cone-shaped micro pin fins. Int. Commun. Heat Mass Transfer 92 (2018) 78–89.
https://doi.org/10.1016/j.icheatmasstransfer.2017.11.004

[18] Li, Y.; Wang, Z.; Yang, J.; Liu, H., Thermal and hydraulic characteristics of microchannel heat sinks with cavities and fins based on field synergy and thermodynamic analysis. Applied Thermal Engineering 175 (2020) 115348.
https://doi.org/10.1016/j.applthermaleng.2020.115348

[19] Li, M.; Gao, X.; Li, H.; Sang, J.; Nie, P.; Fang, W.; Xu, T., Investigation of Flow and Heat Transfer Characteristics in Microchannels with Fins. Machines11 (2023) 154.
https://doi.org/10.3390/machines11020154

[20] Bhatt, H.; Bist, H.; Gola, H.; Zunaid, M., Variation of heat transfer characteristics of a microchannel heat sink with geometry. Mater. Today Proc. 56 (2022) 936–942.https://doi.org/10.1016/j.matpr.2022.02.631

[21] Sadique, H.; Murtaza, Q.; Samsher, Heat transfer augmentation in microchannel heat sink using secondary flows: A review. Int. J. Heat Mass Transfer 194 (2022) 123063.
https://doi.org/10.1016/j.ijheatmasstransfer.2022.123063

[22] Jiang, F.; Drese, K.S.; Hardt, S.; Küpper, M.; Schönfeld, F., Helical flows and chaotic mixing in curved micro channels. AIChE J. 50 (9) (2004) 2297–2305.
https://doi.org/10.1002/aic.10188

[23] Guzniczak, E.; Otto, O.; Whyte, G.; Willoughby, N.; Jimenez, M.; Bridle, H., Deformability-induced lift force in spiral microchannels for cell separation. Lab Chip 20 (3) (2020) 614–625.
DOI: 10.1039/x0xx00000x
[24] Liu, Y.; Jian, Y.; Yang, C.,Electrochemomechanical energy conversion efficiency in curved rectangular nanochannels. Energy 198 (2020) 117401.
https://doi.org/10.1016/j.energy.2020.117401
[25] Rovenskaya, O. I., “Computational Study of 3D Rarefied Gas Flow in Microchannel with 90 Bend.” European Journal of Mechanics. B, Fluids 59 (2016) 7–17.
https://doi.org/10.1016/j.euromechflu.2016.04.008.
[26] Yang, X.; Yao, H.; Zhao, G.; Ameer, G.A.; Sun, W.; Yang, J.; Mi, S., Flexible, wearable microfluidic contact lens with capillary networks for tear diagnostics. J. Mater. Sci. 55 (2020) 9551–9561.
https://doi.org/10.1007/s10853-020-04688-2
[27] Khoshvaght-Aliabadi, M.; Deldar, S.; Salimi, A.; Rashidi, M.M., Effects of cross section geometry on performance of corrugated miniature heat sink: Uniform, convergent, divergent, and hybrid cases. Int. Commun. Heat Mass Transfer 127 (2021) 105269.
https://doi.org/10.1016/j.icheatmasstransfer.2021.105269
[28] Zhang, L.Y.; Duan, R.J.; Che, Y.; Lu, Z.; Cui, X.; Wei, L.C.; Jin, L.W., A numerical analysis of fluid flow and heat transfer in wavy and curved wavy channels. Int. J. Therm. Sci. 171 (2022) 107248.
https://doi.org/10.1016/j.ijthermalsci.2021.107248
[29] Chandratilleke, T.T.; Nadim, N.; Narayanaswamy, R., Vortex structure based analysis of laminar flow behaviour and thermal characteristics in curved ducts. Int. J. Therm. Sci. 59 (2012) 75–86.https://doi.org/10.1016/j.ijthermalsci.2012.04.014
[30] Liu, X.; Fu, Y.; Wang, J.; Zhang, H.; Zhu, J., Investigation on flow and heat transfer in rectangular cross-section sinusoidal channels. Int. J. Therm. Sci. 176 (2022) 107490.
https://doi.org/10.1016/j.ijthermalsci.2022.107490
[31] Mario Di Capua, H.; Escobar, R.; Diaz, A.J.; Guzmán, A.M., Enhancement of the cooling capability of a high concentration photovoltaic system using microchannels with forward triangular ribs on sidewalls. Appl. Energy 226 (2018) 160–180.
https://doi.org/10.1016/j.apenergy.2018.05.052
[32] Liu, X.; Zhang, H.; Zhu, C.; Wang, F.; Li, Z., Effects of structural parameters on fluid flow and heat transfer in a serpentine microchannel with fan-shaped reentrant cavities. Appl. Therm. Eng. 151 (2019) 406–416.
https://doi.org/10.1016/j.applthermaleng.2019.02.033
[33] Li, M.; Gao, X.; Li, H.; Ma, Y.; Sang, J.; Xu, T., Effect of curvature ratio on curved microchannel heat sinks. International Journal of Thermofluids 22 (2024) 100635.
https://doi.org/10.1016/j.ijft.2024.100635
[34] Ansari, M.Q.; Zhou, G., Flow and heat transfer analysis of microchannels structured with rectangular surface roughness. Chemical Engineering & Processing: Process Intensification 156 (2020) 108066.
https://doi.org/10.1016/j.cep.2020.108066

[35] Mandev, E.; Manay, E., Effects of surface roughness in multiple microchannels on mixed convective heat transfer. Applied Thermal Engineering 217 (2022) 119102. https://doi.org/10.1016/j.applthermaleng.2022.119102

[36] Karali, M.A.; Almohammadi, B.A.; Bin Mahfouz, A.S.; Abdelmohimen, M.A.H.; Attia, E.; Refaey, H.A., Effect of surfaces roughness of a staggered tube bank in cross flow with air on heat transfer and pressure drop. Case Studies in Thermal Engineering 43 (2023) 102779. https://doi.org/10.1016/j.csite.2023.102779

[37] Agrawal, Y.; Bhagoria, J.L.; Gautam, A.; Chaurasiya, P.K.; Dhanraj, J.A.; Solomon, J.M.; Salyan, S., Experimental evaluation of hydrothermal performance of solar air heater with discrete roughened plate.Applied Thermal Engineering 211 (2022) 118379. https://doi.org/10.1016/j.applthermaleng.2022.118379

[38] Cahyo, N.; Paryanto, P.; Nugraha, A.D.; Simaremare, A.; Aditya, I.A.; Siregar, B.S.L.; Tauviqirrahman, M. Effect of Engineered Roughness on the Performance of Journal Bearings Lubricated by Bingham Plastic Fluid Using Computational Fluid Dynamics (CFD). Lubricants 2022, 10, 333. https://doi.org/10.3390/ lubricants10120333

[39] Karali, M.A.; Alharthi, M.A.; Refaey, H.A., Influence of using different tapered longitudinal section manifolds in a Z shaped flat plate solar collector on flow distribution uniformity. Case Studies in Thermal Engineering 33 (2022) 101922. https://doi.org/10.1016/j.csite.2022.101922

[40] ANSYS CFX-Solver Theory Guide, ANSYS Inc. R 18.0, 2017.

[41] Lu, H.; Xu, M.; Gong, L.; Duan, X.; Chai, J.C., Effects of surface roughness in microchannel with passive heat transfer enhancement structures. International Journal of Heat and Mass Transfer 148 (2020) 119070.https://doi.org/10.1016/j.ijheatmasstransfer.2019.119070

Submitted: 29.07.2025
Revised: 24.09.2025
Accepted: 12.10.2025